

# Enhancing compressive response of Mg-6Al alloy using Al<sub>2</sub>O<sub>3</sub> nanoparticles

K. Bimla Mardi<sup>1</sup>, A. Mallick<sup>1\*</sup>, A. Rai Dixit<sup>1</sup>, M. Gupta<sup>2</sup>

<sup>1</sup>Department of Mechanical Engineering, Indian Institute of Technology (ISM) Dhanbad, Jharkhand 826004, India

<sup>2</sup>Department of Mechanical Engineering, National University of Singapore,  
9 Engineering Drive 1, Singapore 117576, Singapore

Received 5 February 2018, received in revised form 28 March 2018, accepted 18 April 2018

## Abstract

In this study, Mg-6Al/Al<sub>2</sub>O<sub>3</sub> nanocomposites were synthesized using disintegrated melt deposition technique followed by hot extrusion. Two different amounts of alumina nanoparticles (0.66 and 1.11 wt.%) were added into Mg-6Al matrix. Microstructure and mechanical properties were investigated. Results of XRD analysis revealed that the presence of alumina nanoparticles assisted in randomization of texture (basal to prismatic). The compressive response regarding hardness and compressive strength was assessed using nanoindentation and compressive tests. The results of hardness, modulus of elasticity, compressive strength and the deformation behavior of the composites were compared with pure Mg and Mg-6Al alloy. In all the cases, the composites exhibit better mechanical properties.

Key words: Mg-6Al alloy, Al<sub>2</sub>O<sub>3</sub> nanoparticles, microstructure, compression, nano-indentation

## 1. Introduction

Magnesium (Mg), one of the lightest and the sixth most abundant structural material, is known for energy efficiency and emission reduction primarily in automotive and aviation applications. Other than its low density, Mg exhibits several benefits including excellent castability, good specific strength, high damping capacity, good resistance to electromagnetic radiation, and good machinability. Magnesium requires less energy for mass production of structural equipment as compared to aluminum [1, 2]. However, magnesium-based materials suffer from low corrosion resistance, low ductility and modulus of elasticity, low abrasion resistance and poor creep resistance which limits their use in structural applications. These limitations can be circumvented by the development of new magnesium-based composites and nanocomposites [1, 3–5]. Mg-based alloys and composites are well-addressed by many researchers for improving the mechanical properties along with ductility. The mechanical properties in Mg alloys can be improved by minimizing the percentage of internal defect area using quasi-vacuum casting [6]. Hradilova and Vojtech

[7] have demonstrated that the extrusion process and the addition of small wt.% of Zn and Ca in Mg make significant structural refinement leading to substantial improvement in tensile strength. Further, Li et al. [8] have exposed that continuous variable cross-section direct extrusion (CVCDE) process gives more grain refinement over the conventional extrusion process, and correspondingly the tensile strength can be enhanced more as compared to the ordinary extrusion process.

The rapid development of lightweight Mg-based materials reinforced with nanoparticles is aiming to replace aluminum alloys and steels in electronic, automobile and aviation sectors. In addition to that, hard ceramic nanoparticles in Mg improve the room temperature strength, formability and intrinsically limited ductility [9].

Among the different processing techniques, disintegrated melt deposition (DMD) is one of the most common techniques successfully utilized to synthesize magnesium-based nanocomposites [10–13] for fabricating Mg-based nanocomposites. DMD is a promising technique due to its ability to combine the advantages of spray atomization and deposition technique with that of conventional casting [2, 14]. Hassan and

\*Corresponding author: tel.: +91 9471192246; fax: +92 326 229 6563; e-mail address: [mal123\\_us@yahoo.com](mailto:mal123_us@yahoo.com)

Table 1. The chemical composition of the materials used in this study

| Materials                                       | Mg-Al alloy matrix |                | Reinforcement                         | Particle size<br>(nm) |
|---|--------------------|----------------|---------------------------------------|-----------------------|
|   | Pure Mg (wt.%)     | Pure Al (wt.%) | Al <sub>2</sub> O <sub>3</sub> (wt.%) |                       |
|   | 94                 | 6              |                                       |                       |
| Mg-6Al/0.66 wt.% Al <sub>2</sub> O <sub>3</sub> | 99.34              |                | 0.66                                  | 50                    |
| Mg-6Al/1.11 wt.% Al <sub>2</sub> O <sub>3</sub> | 98.89              |                | 1.11                                  | 50                    |

Gupta [10] compared the microstructures, mechanical properties and coefficients of thermal expansion of Mg/Al<sub>2</sub>O<sub>3</sub> nanocomposite synthesized by DMD and blend-press-sinter powder metallurgy technique. They attributed the uniform distribution of particles by DMD method to optimized stirring, good wetting, the disintegration of melt slurry and dynamic deposition on the steel substrate. In powder metallurgy (PM) high extrusion ratio was responsible for realizing a uniform distribution of particles. Also, superior grain refinement noticed in DMD processed composite was attributed to the uniform distribution of nano-sized reinforcement which acts as nuclei and restricts further grain growth during solidification. Improved microstructural, mechanical and physical properties of Mg/nano-Al<sub>2</sub>O<sub>3</sub> processed by DMD technique was also reported by Hassan and Gupta [11]. They noticed the addition of nanoparticles in Mg matrix led to significant improvement in hardness, elastic modulus, 0.2 % yield strength, ultimate tensile strength (UTS) and ductility. Further, Hassan et al. [12] characterized the effects of the high-temperature tensile behavior of Mg/Al<sub>2</sub>O<sub>3</sub> nanocomposite prepared by DMD method followed by hot extrusion. The experimental results showed the improvement in dimensional stability, grain refinement, inhibited grain growth of Mg matrix during the high-temperature tensile test. Paramsothy et al. [13] produced AZ31/1.5 vol.% Al<sub>2</sub>O<sub>3</sub> nanocomposite by similar fabrication method. They investigated the crystallographic textures and the effect of nanoparticle integration on the enhancement of tensile and compressive properties of AZ31. The mechanical properties such as microhardness, 0.2 % tensile yield strength, UTS enhanced by 30 %, +19 %, +21 % respectively while about 5 % enhancement of yield strength and ultimate strength was observed in compression. Alam et al. [15] developed AZ41 and AZ51 magnesium-based alloy composites containing Al<sub>2</sub>O<sub>3</sub> following the same fabrication route. They investigated the microstructural, mechanical and physical properties of nanocomposites. They observed that the addition of nano-Al<sub>2</sub>O<sub>3</sub> into AZ31 Mg alloy helped to decrease the coefficient of thermal expansion with significant improvement in micro-hardness values and tensile strength. The increase in tensile strength and hardness was attributed to the presence of uniformly distributed intermetallic phase that led to the effective

transfer of applied tensile load.

The results of literature search indicate that no work is conducted so far to determine the compressive response of Mg-6Al based nanocomposites. Accordingly, the primary focus of this study was to develop nanocomposites (Mg-6Al alloy matrix + Al<sub>2</sub>O<sub>3</sub> nanoparticles) using well established DMD method [16]. The fabricated composites were hot extruded and then characterized for their microstructural behavior and compressive properties. The compressive properties were investigated using nanoindentation and compression testing.

## 2. Experimental details

### 2.1. Material composition

In this study, the magnesium turnings (> 99.9 % purity) supplied by ACROS Organics, New Jersey, USA were used as base material. The aluminum lumps with 99.5 % purity (supplied by Alfa Aesar, USA) were used as an alloying element. As a reinforcement, the Al<sub>2</sub>O<sub>3</sub> powder of average particle size 50 nm (> 99.5 % purity) supplied by Baikowski, Japan was mixed at two different weight percents (0.66 and 1.11 %). The chemical composition of the used materials is given in Table 1.

### 2.2. Processing method

The Mg-based metal matrix nanocomposites were synthesized by DMD technique [16]. The process included melting and superheating of magnesium turnings to 750 °C under argon gas atmosphere in a graphite crucible with the addition of 6 wt.% aluminum. The Al<sub>2</sub>O<sub>3</sub> powder, used as reinforcement, was placed in a multi-layered arrangement before heating. The superheated melt slurry was stirred for 5 min at about 450 rpm by mild steel impeller with twin blade of pitch 45° for providing a uniform dispersion of nanoparticles and to ensure temperature homogeneity. The stirrer was coated with Zirtex 25 (86 % ZrO<sub>2</sub>, 8.8 % Y<sub>2</sub>O<sub>3</sub>, 3.6 % SiO<sub>2</sub>, 1.2 % K<sub>2</sub>O and Na<sub>2</sub>O, and 0.3 % trace inorganic) to prohibit the iron contamination. The molten metal was then discharged from the crucible through bottom pouring (10 mm diameter

orifice) and before depositing into the substrate, the melt was disintegrated by two jets of argon gas (flow rate  $25 \text{ l min}^{-1}$ ) oriented normal to the melt stream. The distance between the base of the substrate and disintegration point was set as 500 mm. An ingot of 40 mm diameter was then collected from the metallic substrate. The monolithic magnesium ingot was prepared by similar route except for the addition of reinforcement.

The deposited preforms were machined to produce a cylindrical billet of 36 mm diameter and 45 mm length. The billets were hot extruded at  $350^\circ\text{C}$ . Before extrusion, the samples were thermally treated at  $350^\circ\text{C}$  for one hour and then extruded with an extrusion ratio of 20:1 to produce 8 mm diameter cylindrical rods of the composites and pure Mg.

### 2.3. Density and porosity measurement

The density of polished samples of the monolithic Mg and nanocomposites was measured by Archimedes principle to quantify the volume fraction of porosity. The distilled water was used as the immersion fluid. The densities were measured by weighing polished disc of the extruded rod in the air as well as in immersion fluid. For measurement Sartorius BSA4202S-CW weighing machine was used with an accuracy of  $\pm 0.0001 \text{ g}$ . Theoretical densities were calculated by assuming that materials are fully dense and there is no interfacial reaction between the Mg-6Al matrix alloy and alumina. Law-of-mixture was applied for theoretical density calculations. The volume fractions of porosity were calculated by using values of theoretical and experimental density.

### 2.4. Microstructural characterization

The microstructural studies were carried out on metallographically polished samples of the extruded rods of composites and monolithic Mg. The grain morphology, pores and the presence of reinforcement were investigated. For microstructural observation, the samples were machined and cut perpendicular to the direction of extrusion. Field Emission Scanning Electron Microscope (FESEM) equipped with Energy Dispersive Spectroscopy (EDS), model Supra 55 (Carl Zeiss, Germany) was employed. TEM analysis of the composites was performed to quantify the microstructural features. The samples for TEM analysis were prepared by ion milling using the operating voltages of 6–10 kV at the inclination angle of  $10^\circ$  under a vacuum environment.

### 2.5. X-Ray diffraction analysis

X-ray diffraction (XRD) analyses of pure Mg and nanocomposites were conducted on automated Bruker

D8 Discover diffractometer. The 5 mm height cylindrical extruded samples were confirmed to be flattened, polished and ultrasonically cleaned before doing XRD. The XRD patterns were collected using  $\text{CuK}\alpha$  radiation ( $\lambda = 0.1540 \text{ nm}$ ) with the scanning speed  $0.5 \text{ s/step}$ . The Bragg's angles (2-Theta) from  $20\text{--}80^\circ$  were scanned for all the samples, and the step size was  $0.02^\circ$ . The values of d-spacing or interplanar spacing from the digital output at different Bragg's angle were compared with the standard values from pcpdfwin JCPDS (Joint Committee on Powder Diffraction Standards) software for the presence of Mg and related intermetallic phases.

### 2.6. Mechanical properties

The mechanical properties include the measurement of hardness, Young's modulus, yield strength and compressive strength. The hardness and Young's modulus were measured from the nanoindentation test. The compressive and yield strength were estimated from the compressive test. Nanoindentation tests were performed on the mirror polished samples using MTS/Agilent at a constant strain rate of  $0.05 \text{ s}^{-1}$  to obtain maximum penetration depth of about 2000 nm. A Berkovich USA with XP-nanoindenter in continuous stiffness mode (CSM) was employed for the nanoindentation test. The indenter with effective cone angle  $70.3^\circ$  was used for indentation. The indentation data was statistically evaluated from ten indentations at a different position of each sample. The compressive tests were performed on the flat 8 mm diameter and 8 mm height cylindrical samples in accordance with ASTM D695 at room temperature using HOUNSFIELD H50KS machine. A constant strain rate,  $\dot{\epsilon} = 0.833 \times 10^{-4} \text{ s}^{-1}$ , was considered for all the samples. For ensuring consistency, five tests were repeated for each category of the samples.

### 2.7. Fracture behavior

Fracture surfaces of the failed samples after compression were examined to understand insight into fracture mechanisms of pure Mg and composite samples. Field emission scanning electron microscopy (FESEM) Supra 55 (Carl Zeiss, Germany) was used for this purpose.

## 3. Results and discussion

### 3.1. Density and porosity measurements

The theoretical and experimental values of density and the volume fractions of porosity are listed in Table 2. It can be seen that the density of the nanocomposites increases insignificantly with the addition of

Table 2. Results of density and porosity measurement of pure Mg and nanocomposites

| Compositions                             | Density ( $\text{g cm}^{-3}$ ) |               | Porosity (%) |
|--|--------------------------------|---------------|--------------|
|  | Theoretical                    | Experimental* |              |
| Pure Mg                                  | 1.7398                         | 1.7391        | 0.04         |
| Mg-6Al/0.66 wt.% $\text{Al}_2\text{O}_3$ | 1.7523                         | 1.7512        | 0.06         |
| Mg-6Al/1.11 wt.% $\text{Al}_2\text{O}_3$ | 1.7673                         | 1.7655        | 0.10         |

\*Three tests on randomly selected three specimens were done for each material.

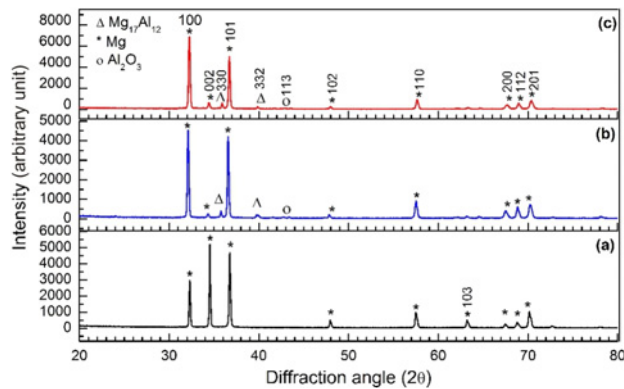


Fig. 1. X-Ray diffraction pattern of: (a) pure Mg, (b) Mg-6Al/0.66 wt.%  $\text{Al}_2\text{O}_3$ , and (c) Mg-6Al/1.11 wt.%  $\text{Al}_2\text{O}_3$ .

nano- $\text{Al}_2\text{O}_3$  particles. The increase in density is attributed to the higher density of  $\text{Al}_2\text{O}_3$  ( $3.96 \text{ g cm}^{-3}$ ) [2, 15] and Al ( $2.7 \text{ g cm}^{-3}$ ) when compared to the density of Mg ( $1.74 \text{ g cm}^{-3}$ ). The theoretical and experimental densities are found to be very close. The minimal porosity in the present materials suggested the appropriateness of the experimental parameters used in this study and can principally be attributed to (a) good compatibility between Mg-6Al matrix alloy and nanoparticles of  $\text{Al}_2\text{O}_3$  [16], (b) suitable sintering conditions, (c) suitable disintegration parameters and (d) appropriate selection of extrusion ratio. The maximum porosity level, 0.10 %, was observed in the composite with 1.11 wt.%  $\text{Al}_2\text{O}_3$ . The marginal increase in the amount of porosity with  $\text{Al}_2\text{O}_3$  nanoparticles may be attributed to the nucleation or the coalescence of pores at the  $\text{Al}_2\text{O}_3$  particulate surfaces [17].

### 3.2. X-ray diffraction analysis

The XRD patterns of extruded samples of pure Mg and nanocomposites of Mg-6Al matrix alloy are illustrated in Fig. 1. The XRD pattern of monolithic Mg samples shows sharp peaks of HCP Mg crystal at  $32.30^\circ$ ,  $34.55^\circ$  and  $36.76^\circ$  diffraction angles representing the prismatic plane (1 0 0), basal plane (0 0 2) and pyramidal plane (1 0 1) [18]. The presence of only Mg phase in Fig. 1a confirms the material is pure Mg. The XRD spectra of composite samples with rein-

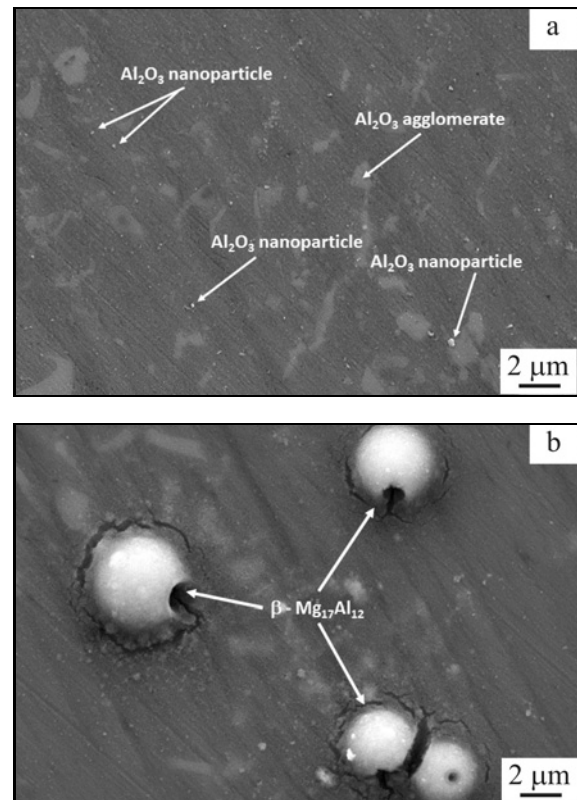


Fig. 2. FESEM micrograph of Mg-6Al/1.11 wt.%  $\text{Al}_2\text{O}_3$  showing: (a) the presence of  $\text{Al}_2\text{O}_3$  and their cluster and (b) formation of  $\text{Mg}_{17}\text{Al}_{12}$  second phase particles.

forcement 0.66 wt.%  $\text{Al}_2\text{O}_3$  and 1.11 wt.%  $\text{Al}_2\text{O}_3$  are presented in Figs. 1b,c. The peak of  $\text{Al}_2\text{O}_3$  at  $43.40^\circ$  diffraction angles suggested that nano-sized alumina particles were present in Mg-6%Al matrix. A reduction in intensity of basal plane of Mg peak at  $34.33^\circ$  in the composite samples was due to the addition of reinforcement that indicated the randomization of texture [19, 20]. The absence of Al peak revealed that Al completely dissolved into Mg during DMD process. The XRD analysis of composite samples revealed the presence of  $\beta\text{-Al}_{12}\text{Mg}_{17}$  intermetallic phase which is an equilibrium phase in Mg-Al binary system.

### 3.3. Microstructural study

Figure 2 shows the FESEM micrographs of the

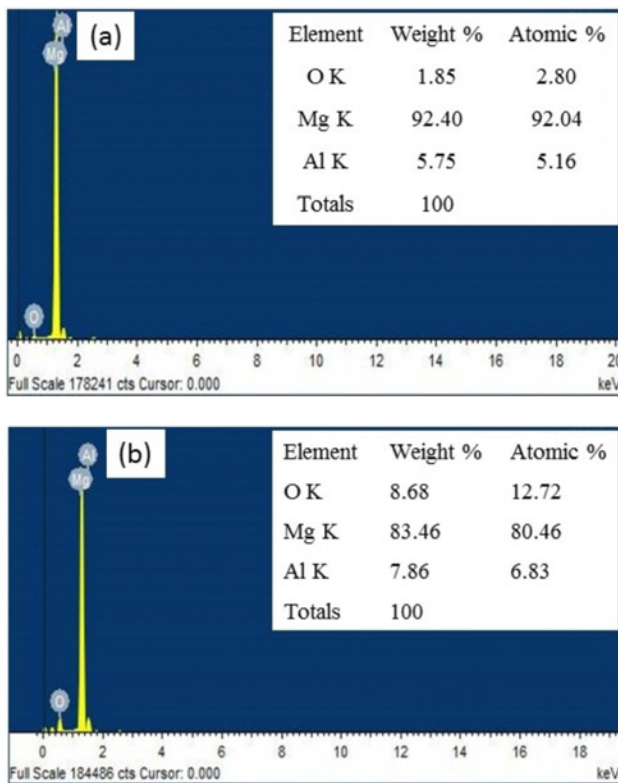


Fig. 3. EDS analysis of the extruded nanocomposites: (a) Mg-6Al/0.66 wt.%  $\text{Al}_2\text{O}_3$  and (b) Mg-6Al/1.11 wt.%  $\text{Al}_2\text{O}_3$ .

polished Mg-6Al/1.1 wt.%  $\text{Al}_2\text{O}_3$  nanocomposite. It could be seen that the nano-sized  $\text{Al}_2\text{O}_3$  dispersed with good interfacial integrity (Fig. 2a). The micrograph also revealed the occurrence of agglomeration of  $\text{Al}_2\text{O}_3$  in the composite. The agglomeration of  $\text{Al}_2\text{O}_3$  in the alloy matrix could be due to the large gap in the matrix and particulate powder size. The well-defined large secondary phase  $\text{Mg}_{17}\text{Al}_{12}$  particles are observed in the micrograph of composite (Fig. 2b). This result suggests that the formation of  $\beta\text{-Mg}_{17}\text{Al}_{12}$  phase is the result of interaction between Mg and Al during the solidification of Mg-6Al alloys. It is expected that the fine second phase particles and  $\text{Al}_2\text{O}_3$  nano-reinforcement inhibit the grain boundary migration, and thereby controlling the grain growth during the recrystallization. The reduction of grain size through grain refinement in the composites as compared to monolithic Mg processed by the same route is due to the formation of  $\text{Mg}_{17}\text{Al}_{12}$  and the presence of nanoparticles of  $\text{Al}_2\text{O}_3$  in the composite. The EDX analysis as shown in Fig. 3 reveals the percentage of the compositions present in the nanocomposites. As expected, magnesium, aluminum and oxygen were detected in the spectrum of EDX. The percentage of Mg in composite with 1.11 wt.% of reinforcement is found to be less as compared to composites with 0.66 wt.%

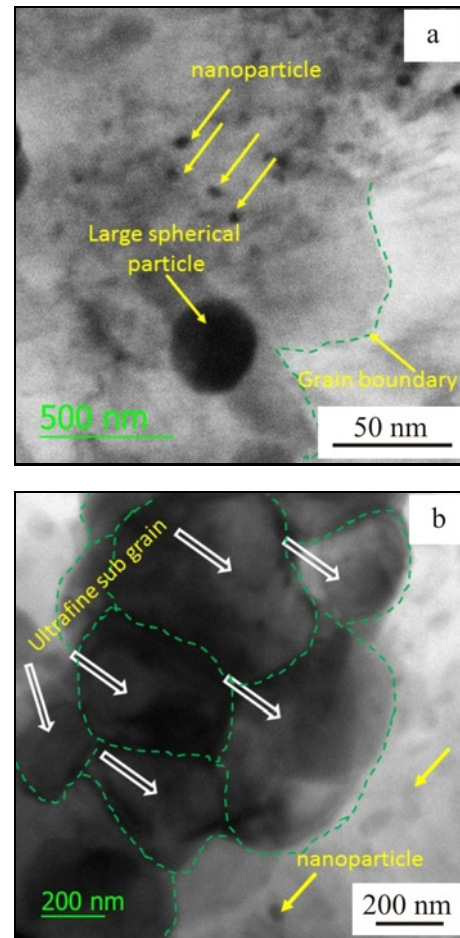


Fig. 4. TEM images of: (a) Mg-6Al/0.66 wt.%  $\text{Al}_2\text{O}_3$  and (b) Mg-6Al/1.11 wt.%  $\text{Al}_2\text{O}_3$ .

of reinforcement. Relatively higher % of oxygen is attributed in the composites with 1.11 wt.% of  $\text{Al}_2\text{O}_3$  as compared to 0.66 wt.% of  $\text{Al}_2\text{O}_3$ . The result may be due to the presence of higher volume percentage of  $\text{Al}_2\text{O}_3$  and the formation of oxide particles in Mg-6Al/1.11 wt.%  $\text{Al}_2\text{O}_3$  composite. Figure 4 represents the TEM micrographs of the composites reinforced with 0.66 and 1.11 wt.%  $\text{Al}_2\text{O}_3$  nanoparticles. The results show bigger grains along with smaller subgrains of submicron size. Isolated presence of nano-ceramic particles of  $\text{Al}_2\text{O}_3$  was observed in both the composite samples. The grain boundary region appears to be almost clean and dislocation free. The TEM results with higher weight fraction (1.11 wt.%) of the nano-reinforcement show the formation of subgrains indicated by slight color difference and very fine grain boundaries due to small misorientation angles between them.

### 3.4. Nanoindentation results

The results of nanoindentation tests of the com-

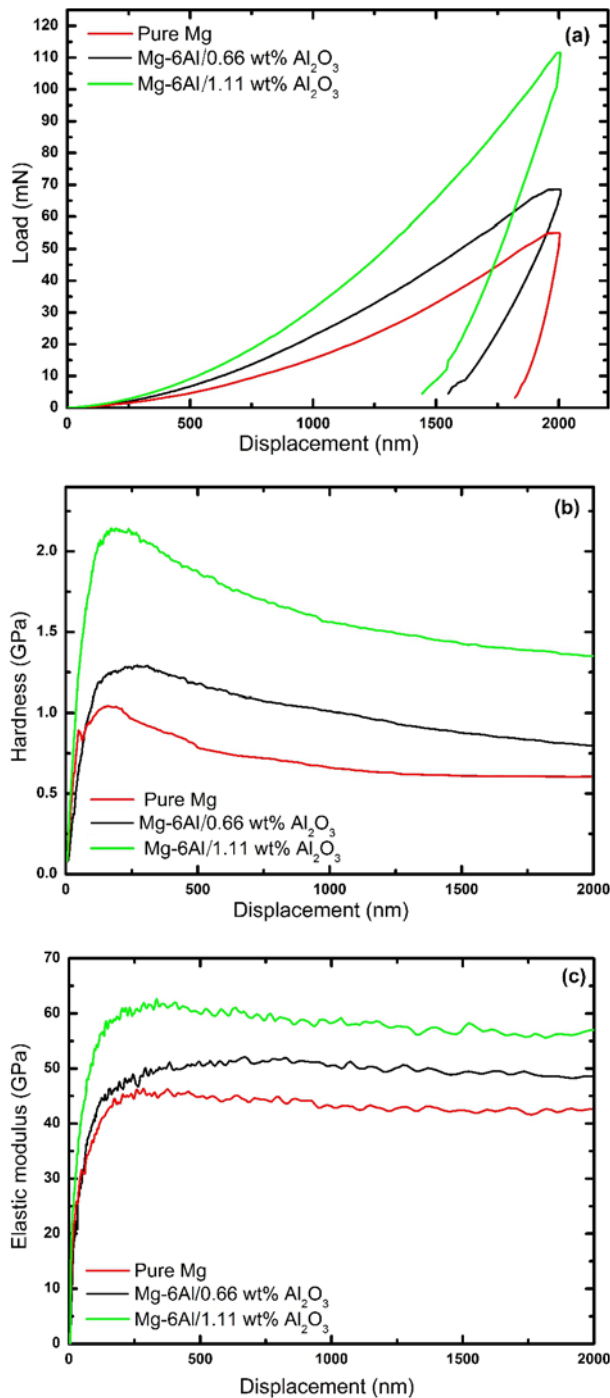


Fig. 5. Nanoindentation results showing variation in: (a) load, (b) hardness, and (c) elastic modulus of nanocomposites and pure Mg.

posites and monolithic Mg are presented in Fig. 5. The load-displacement curves of indentation test are depicted in Fig. 5a and the corresponding variation of hardness and elastic modulus values are presented in Fig. 5b and Fig. 5c respectively. The specimens undergo plastic deformation with a depth of indenter penetration of about 2000 nm. In Fig. 5a,

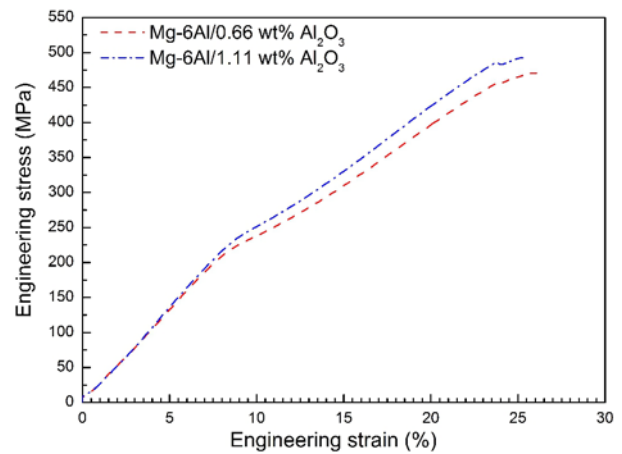


Fig. 6. Stress-strain behavior of the synthesized nanocomposites under compressive loading.

it can be seen that the indentation loads 110, 60 and 50 mN were applied in Mg-6Al/1.11 wt.%  $\text{Al}_2\text{O}_3$ , Mg-6Al/0.66 wt.%  $\text{Al}_2\text{O}_3$  and monolithic Mg samples to achieve the same indentation depth (about  $\sim 2000$  nm). Correspondingly, the maximum hardness values were obtained in the composites with 1.11 wt.%  $\text{Al}_2\text{O}_3$  nanoparticles and followed by composites with 0.66 wt.%  $\text{Al}_2\text{O}_3$  nanoparticles and pure Mg. The variation of elastic modulus as a function of indentation depth reveals that maximum elastic modulus is associated with Mg-6Al/1.11 wt.%  $\text{Al}_2\text{O}_3$  composite and followed by Mg-6Al/0.66 wt.%  $\text{Al}_2\text{O}_3$  composite and pure Mg samples. The range of hardness values and elastic modulus is presented in Table 3. It could be seen that hardness is enhanced in Mg-6Al/0.66 wt.%  $\text{Al}_2\text{O}_3$  and Mg-6Al/1.11 wt.%  $\text{Al}_2\text{O}_3$  composites in the range of 33–50 % and 125–130 % when compared to pure Mg sample. The elastic modulus is increased by about 11 and 19 % in Mg-6Al/0.66 wt.%  $\text{Al}_2\text{O}_3$  and Mg-6Al/1.11 wt.%  $\text{Al}_2\text{O}_3$  composites. These results reveal that the improvement in hardness and elastic modulus in the composites is due to the presence of reinforcement of  $\text{Al}_2\text{O}_3$  nanoparticles. The unloading curves of nanoindentation test describe the elastic recovery of the materials. The elastic recovery was measured by the change in indentation depth at maximum load ( $h_{\max}$ ) to a final depth of indentation ( $h_f$ ) following  $\{(h_{\max} - h_f) \times 100/h_{\max}\}$  relationship. The maximum recovery, about 27.3 and 21.8 %, was observed in Mg-6Al/1.11 wt.%  $\text{Al}_2\text{O}_3$  and Mg-6Al/1.11 wt.%  $\text{Al}_2\text{O}_3$  samples. Only 8.75 % elastic recovery was observed in monolithic Mg sample.

### 3.5. Compressive properties

Figure 6 represents the typical compressive stress-strain curves of extruded samples of the composites at room temperature. As apparent from the results, the

Table 3. Results of nanoindentation experiments on pure Mg and nanocomposites

| Material  | Hardness (GPa) | Elastic modulus (GPa) |
|---|----------------|-----------------------|
| Pure Mg   | 0.6–0.8        | 43–45                 |
| Mg-6Al/0.66 wt.% Al <sub>2</sub> O <sub>3</sub> | 0.8–1.2        | 47–51                 |
| Mg-6Al/1.11 wt.% Al <sub>2</sub> O <sub>3</sub> | 1.4–1.8        | 56–62                 |

Table 4. Results of CYS, UCS and failure strain at room temperature compression testing

| Material  | Strain rate (s <sup>-1</sup> ) | CYS (MPa) | UCS (MPa) | Failure strain (%) |
|---|--------------------------------|-----------|-----------|--------------------|
| Pure Mg*  | 0.833 × 10 <sup>-4</sup>       | 81 ± 3    | 368 ± 11  | 20.1 ± 0.9         |
| Mg-6Al*   | 0.833 × 10 <sup>-4</sup>       | 169 ± 19  | 464 ± 21  | 20.2 ± 3.6         |
| Mg-6Al/0.66 wt.% Al <sub>2</sub> O <sub>3</sub> | 0.833 × 10 <sup>-4</sup>       | 221 ± 4   | 470 ± 3   | 25.8 ± 0.4         |
| Mg-6Al/1.11 wt.% Al <sub>2</sub> O <sub>3</sub> | 0.833 × 10 <sup>-4</sup>       | 243 ± 6   | 496 ± 2   | 25.4 ± 0.9         |

\*The CYS, UCS and failure strain values of pure Mg and Mg-6Al alloy are compiled from references given in [21].

addition of alumina nanoparticles has a significant effect on the compressive strength. The results reveal that the composite with 1.11 wt.% Al<sub>2</sub>O<sub>3</sub> nanoparticles leads to higher compressive strength as compared to the composite with 0.66 wt.% Al<sub>2</sub>O<sub>3</sub> nanoparticles. The results of compressive yield strength (CYS), compressive ultimate strength (CUS) and failure strain of the composites are compared with the pure Mg and Mg-6Al alloy prepared by the same route [21] in Table 4. It can be seen that the addition of 0.66 wt.% Al<sub>2</sub>O<sub>3</sub> nanoparticle as reinforcement leads to an increase in CYS, UCS and failure strain by about 169, 31 and 35 % as compared to pure Mg and about 30 %, 1.3 % and 27.8 % as compared to Mg-6Al alloy. The CYS, UCS and failure strain in Mg-6Al/1.11 wt.% Al<sub>2</sub>O<sub>3</sub> nanocomposite increase by about 196, 38, and 33 % as compared to pure Mg and about 43, 6.8, and 25.89 % as compared to Mg-6Al alloy. These results reveal that small percentage of nanoparticles of Al<sub>2</sub>O<sub>3</sub> significantly contribute to improvement in the strength and ductility. The enhancement in strength can be due to a combination of various strengthening mechanisms such as dislocation strengthening, grain boundary pinning, particle strengthening and CTE/E mismatch strengthening activated by the induction of hard ceramic nanoparticles into a soft matrix. Microstructural reasons for these mechanisms to be activated include a) uniform distribution of ceramic particles, and b) good matrix-particle interfacial integrity.

### 3.6. Fractography

The fracture morphology of the deformed samples under compressive loading is illustrated in Fig. 7. All the samples are split into two parts. It is noticed that the fracture surfaces of all the samples are inclined at an angle of ~45° to the compression loading direction. The microstructural analysis of the deformed

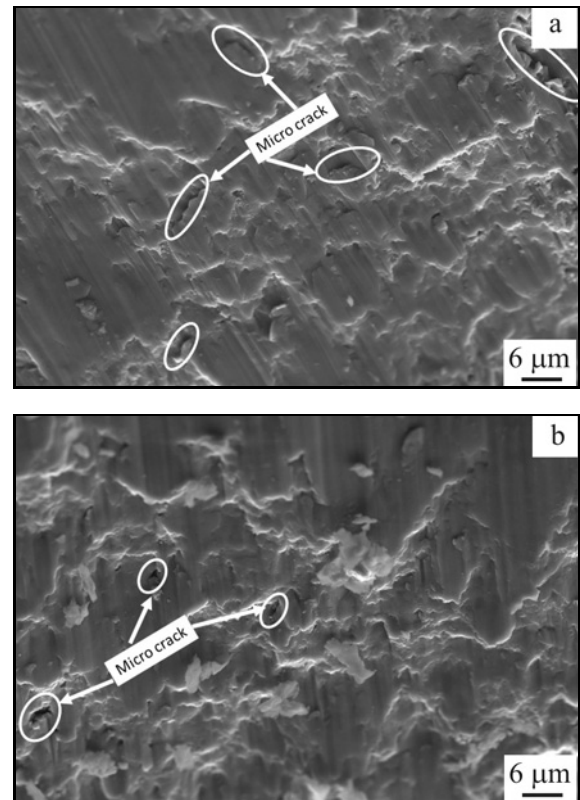


Fig. 7. Fractured surfaces of the deformed samples after compression test of: (a) Mg-6Al/0.66 wt.% Al<sub>2</sub>O<sub>3</sub> and (b) Mg-6Al/1.11 wt.% Al<sub>2</sub>O<sub>3</sub>.

fracture surfaces revealed the presence of winding torn edges with varying degree of shear band formation. The maximum stresses were parallel to the plane of the fracture surface that led to the localized strain and shear band formation. Few secondary cracks were observed, and the samples experienced shear mode fracture.

#### 4. Conclusions

Mg-6Al alloy reinforced with Al<sub>2</sub>O<sub>3</sub> nano-sized particles was successfully synthesized by DMD method followed by hot extrusion. Simultaneously, the microstructure, nanoindentation and compression properties were investigated. From this study, following conclusions can be drawn:

1. The incorporation of Al<sub>2</sub>O<sub>3</sub> nanoparticles to the Mg-6Al alloy is capable of simultaneously and considerably improving strength along with ductility of matrix alloy.

2. The microstructural study revealed the reduction of grain size due to the formation of  $\beta$ -Al<sub>12</sub>Mg<sub>17</sub> phase and presence of Al<sub>2</sub>O<sub>3</sub> nanoparticles. The bigger grain along with the formation of subgrains of sub-micron size was also observed in Mg-6Al/1.11 wt.% Al<sub>2</sub>O<sub>3</sub> composite.

3. The nanoindentation results revealed that the hardness and modulus of the pure Mg increased with Al<sub>2</sub>O<sub>3</sub> nanoparticles. The increment in hardness values was observed in 33–50% range for Mg-6Al/0.66 wt.% Al<sub>2</sub>O<sub>3</sub> and 125–130% for Mg-6Al/1.11 wt.% Al<sub>2</sub>O<sub>3</sub> as compared to pure Mg.

4. The compressive results conclude that the incorporation of a small fraction of Al<sub>2</sub>O<sub>3</sub> nanoparticles to Mg-6Al matrix alloy significantly improves the compressive properties. The improvement in CYS, UCS and failure strain in Mg-6Al/1.11 wt.% Al<sub>2</sub>O<sub>3</sub> nanocomposite is about 43, 6.8, and 25.89% as compared to Mg-6Al alloy.

#### References

- [1] Gupta, M., Wong, W. L. E.: *Mater. Charact.*, 105, 2015, p. 30. [doi:10.1016/j.matchar.2015.04.015](https://doi.org/10.1016/j.matchar.2015.04.015)
- [2] Nguyen, Q. B., Gupta, M.: *Alloy Compd.*, 459, 2008, p. 244. [doi:10.1016/j.jallcom.2007.05.038](https://doi.org/10.1016/j.jallcom.2007.05.038)
- [3] Goh, C. S., Wei, J., Lee, L. C., Gupta, M.: *Nanotechnology*, 17, 2006, p. 7. [doi:10.1088/0957-4484/17/1/002](https://doi.org/10.1088/0957-4484/17/1/002)
- [4] Friedrich, H. E., Mordike, B. L.: *Magnesium Technology*. Berlin, Heidelberg, Springer 2006. [doi:10.1007/3-540-30812-1\\_6](https://doi.org/10.1007/3-540-30812-1_6)
- [5] Mardi, K. B., Dixit, A. R., Mallick, A., Pramanik, A., Balloková, B., Hvizdos, P., Foldyna, J., Scucka, J., Hlavacek, P., Zelenak, M.: *Mater. Manuf. Proc.*, 32, 2017, p. 1707. [doi:10.1080/10426914.2017.1279306](https://doi.org/10.1080/10426914.2017.1279306)
- [6] Huang, S. J., Lin, C. C., Shiou, F. J., Huang, J. Y.: *Kovove Mater.*, 55, 2017, p. 343. [doi: 10.4149/km-2017-5-343](https://doi.org/10.4149/km-2017-5-343)
- [7] Hradilova, M., Vojtech, D.: *Kovove Mater.*, 52, 2014, p. 361.
- [8] Li, F., Shi, W., Hu, Z. L., Zeng, X.: *Kovove Mater.*, 53, 2015, p. 1. [doi: 10.4149/km-2015-1-1](https://doi.org/10.4149/km-2015-1-1)
- [9] Hassan, S. F., Paramsothy, M., Patel, F., Gupta, M.: *Mater. Sci. Eng. A*, 558, 2012, p. 278. [doi:10.1016/j.msea.2012.08.002](https://doi.org/10.1016/j.msea.2012.08.002)
- [10] Hassan, S. F., Gupta, M.: *Comp. Struct.*, 72, 200, p. 19. [doi:10.1016/j.compstruct.2004.10.008](https://doi.org/10.1016/j.compstruct.2004.10.008)
- [11] Hassan, S. F., Gupta, M.: *Metall. Mater. Trans. A*, 36, 2005, p. 2253. [doi:10.1007/s11661-005-0344-4](https://doi.org/10.1007/s11661-005-0344-4)
- [12] Hassan, S. F., Tan, M. J., Gupta, M.: *Mater. Sci. Eng. A*, 486, 2008, p. 56. [doi:10.1016/j.msea.2007.08.045](https://doi.org/10.1016/j.msea.2007.08.045)
- [13] Paramsothy, M., Hassan, S. F., Srikanth, N., Gupta, M.: *Mater. Sci. Eng. A*, 527, 2009, p. 162. [doi:10.1016/j.msea.2009.07.054](https://doi.org/10.1016/j.msea.2009.07.054)
- [14] Gupta, M., Lane, C., Lavernia, E. J.: *Scripta Metall.*, 26, 1992, p. 825. [doi:10.1016/0956-716X\(92\)90446-L](https://doi.org/10.1016/0956-716X(92)90446-L)
- [15] Alam, E. Md., Han, S., Nguyen, Q. B., Hamouda, A. M. S., Gupta, M.: *J. Alloy Compd.*, 509, 2011, p. 8522. [doi:10.1016/j.jallcom.2011.06.020](https://doi.org/10.1016/j.jallcom.2011.06.020)
- [16] Hassan, S. F., Gupta, M.: *Mater. Sci. Eng. A*, 425, 2006, p. 22. [doi:10.1016/j.msea.2006.03.029](https://doi.org/10.1016/j.msea.2006.03.029)
- [17] Sajjadi, S. A., Ezatpour, H. R., Parizi, M. T.: *Mater. Des.*, 34, 2012, p. 106. [doi:10.1016/j.matdes.2011.07.037](https://doi.org/10.1016/j.matdes.2011.07.037)
- [18] Kumar, A., Tun, K. S., Kohadkar, A. D., Gupta, M.: *Metals*, 7, 2017, p. 104. [doi:10.3390/met7030104](https://doi.org/10.3390/met7030104)
- [19] Mallick, A., Tun, K. S., Vedantam, S., Gupta, M.: *J. Mater. Sci.*, 45, 2010, p. 3058. [doi:10.1007/s10853-010-4312-z](https://doi.org/10.1007/s10853-010-4312-z)
- [20] Mallick, A., Vedantam, S., Li, L.: *Mater. Sci. Eng. A*, 515, 2009, p. 14. [doi:10.1016/j.msea.2009.03.002](https://doi.org/10.1016/j.msea.2009.03.002)
- [21] Seetharaman, S., Blawert, C., Milton Ng, B., Wong, W. L. E., Goh, C. S., Hort, N., Gupta, M.: *J. Alloy Compd.*, 648, 2015, p. 759. [doi:10.1016/j.jallcom.2015.05.284](https://doi.org/10.1016/j.jallcom.2015.05.284)